IEEE Access
Multidisciplinary | Rapid Review | Open Access Journal

Received 23 April 2023, accepted 28 May 2023, date of publication 31 May 2023, date of current version 7 June 2023.

Digital Object Identifier 10.1109/ACCESS.2023.3281740

RESEARCH ARTICLE

A Novel Piezo Inertia Actuator Inspired by Motion Mode of Steam Train's Transmission Mechanism

PINGPING SUN, HUAN YU, AND HAOZHEN ZHANG
School of Physics and Information Engineering, Jiangsu Second Normal University, Nanjing 211200, China
Corresponding author: Pingping Sun (sunpingping123@jssnu.edu.cn)

This work was supported in part by the specialized research fund under Grant 923801.

ABSTRACT Previously reported inertia actuators mostly have the problem of greater deviations between positive and reverse speeds. To solve this problem, we have developed a novel piezo inertia actuator with a similar structure, inspired by the motion mode of the steam train's transmission mechanism. Based on the inertia principle, a saw-tooth waveform voltage is used to drive the actuator. The aim of this study is to report the model design, working principle and the output characteristics experiment of the designed actuator. The prototype is fabricated for testing of mechanical properties. Experiments indicate that the positive and reverse average speeds are 12.59 mm/s and 11.99 mm/s, respectively, with a deviation rate of 4.9%, which is much lower than those of previous actuators. Finally, the experiment proves the effectiveness of the novel piezo inertia actuator inspired by the motion mode of the steam train's transmission mechanism.

INDEX TERMS Piezo actuator, steam train, inertia actuator, transmission mechanism.

I. INTRODUCTION

In the early 19th century, the invention and application of the steam engine, a new power machine, ushered in the age of steam. The train, the ship and other machines could be driven by a steam engine. It brought convenience to people and symbolized advancement of human civilization. A century later, another transition in human engineering and technology development occurred – a transition from the steam age to the electrical age. Electromagnetic generators and motors replaced clumsy steam engines in some certain fields. Compared with steam engines, electromagnetic devices feature small sizes, clean, pollution-free and convenient operations, and high output power, used in a wide variety of applications.

In the decades that followed, the piezo actuators developed rapidly and were used extensively as a novel type of actuator. Unlike conventional motors which are electromagnetically driven, the actuator utilizes the converse piezoelectric effect and has the benefits of a flexible structure, fast responses, power off self-locking, freedom from magnetic field interference, and accurate movement, etc., in addition to the characteristics of low temperature resistance and good vacuum adaptation in the space environment. Under the operating principle, many piezo actuators with various structures and working modes were developed, and they can be classified into three types: ultrasonic actuators, Spanworm actuators and inertia actuators. Ultrasonic actuators [1], [2], [3], [4], [5], [6] make use of the stator's vibration at ultrasonic frequency. The vibrational energy of the elastic stator is converted into the linear motion or rotating motion of the rotor by friction. However, the operating frequency of ultrasonic motor is very susceptible to the environmental temperature and in result the output characteristics of the motor are extremely unstable. Spanworm actuators [7], [8], [9], [10] usually imitate the crawl mode of insects in nature, with multiple sets of parallel piezo-stack that serve the function of insect legs. However, these motors require a complex control method and are more demanding in terms of part accuracy and assembly. In the case of inertia actuators [11], [12], [13], [14], [15], [16], the inertia of a slide guide is used to drive in step motion through continuous friction contact. Typically, a single piezo-stack is used to achieve positive and reverse motion.

Compared with other motors, the inertia motors possess the inherent advantages of a compact construction and a simple control method and have attracted wide attention from

The associate editor coordinating the review of this manuscript and approving it for publication was Michail Kiziroglou.

researchers around the world. However, a problem exists in reported actuators – severe inconsistency between the positive and reverse velocities at the identical driving frequency and voltage. The velocity deviation can be used to indicate the degree of difference between positive and reverse velocities. Here, the velocity deviation β can be expressed by equation (1), where V_F and V_B denote the positive and reverse velocities, respectively.

$$\beta = \frac{2\,|V_F - V_B|}{V_F + V_B} \tag{1}$$

Numerous research workers have carried out a range of studies and improvements in that respect [17], [18], [19]. For example, Li et al. [20] proposed a compact positioning platform driven by the piezo-stack, with the maximum positive and reverse velocities of 1.499 mm/s and 1.18 mm/s and a velocity deviation of 23.8%. Wang et al. [21] presented a novel linear inertia actuator which imitated skateboarding movement, with a velocity deviation of 27.67%. In [22], by using two flexible hinges, the actuator is capable of bidirectional motion. The velocity deviation is 15.17% for positive and reverse velocities of 2.01 mm/s and 2.34 mm/s. However, most of the previous structures of inertial actuators adopt an asymmetric flexible hinge structure, which realizes parasitic motion through different stiffness on both sides of the structure. Because the piezo-stack is embedded into the flexible hinge structure by a certain preloading method, the internal stress of the assembly will cause deformation of the flexible hinge, resulting in a large deviation between the forward and reverse movement speed of the actuator. For the flexible hinge structure of the designed actuator, the deformation of the flexible hinge structure caused by the internal stress of the assembly can still maintain the best driving effect.

In order to reduce the deviation, we have designed a novel piezo inertia actuator, which imitates the motion mode of the steam train's transmission mechanism. The flexible hinge structure of the designed actuator has the same stiffness on both sides and is compact. Inspired by the unique movement mode of the steam train's transmission mechanism, the internal stress will not cause a large deviation between the forward and reverse movement speed of the actuator.

II. STRUCTURES AND MATERIALS

Figure.1 shows the section of a traditional steam train, which consists of four parts: a body, wheels, a steam engine and the transmission mechanism. The steam engine converts the energy of steam into the reciprocating power of the piston, which is then transformed into rotary motion of the wheels through the transmission mechanism. Therefore, the transmission mechanism not only plays the role of energy transformation, but also can effectively transfer the mechanical work.

The study focuses on the motion mode of the steam train's transmission mechanism in the design of a piezo inertia actuator with a similar structure. Figure.2 is a schematic diagram of the steam train's transmission mechanism, which has two

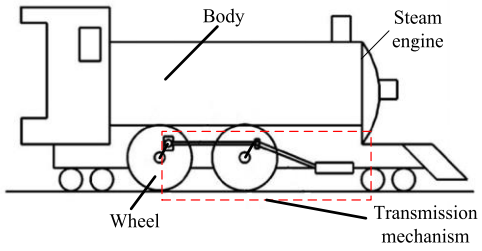

FIGURE 1. Appearance of the steam train.

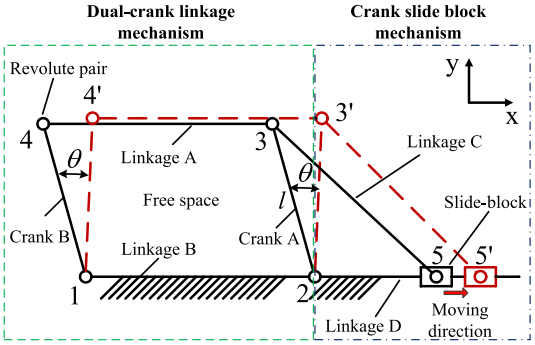

FIGURE 2. Schematic diagram of the steam train's transmission mechanism.

components: a dual-crank linkage mechanism and a crank slide-block mechanism. The dual-crank linkage mechanism resembles a parallelogram, while the crank slide-block mechanism resembles a triangle. The dual-crank linkage mechanism contains two cranks A and B, two linkages A and B and four revolute pairs. The crank slide-block mechanism contains one crank A, two linkages C and D and three revolute pairs. The two mechanisms are connected by one crank A and two revolute pairs 2 and 3. The linkages B and D are completely fixed in two mechanisms. The slide-block and the cranks act as the piston and wheels, respectively. When the slide-block moves forward by some distance, two cranks A and B will rotate at the same angle around the revolute pairs 1 and 2, respectively, and linkage C will rotate and translate to the place 3′-5′ and simultaneously, linkage A will translate to the place 3′-4′. According to an observation of the motion trajectory of linkage A, the displacement in the x-direction is much greater than that in the y-direction.

Given the above, we choose the dual-crank linkage mechanism and the crank slide-block mechanism as the main configuration of the actuator. Given the spacious interior of the dual-crank linkage mechanism, a novel idea is to put the crank slide-block mechanism into the dual-crank linkage mechanism. That can compact the new actuator structure and reduce the actuator size.

The new actuator with a similar structure is shown in Figure 3, whose design is based on the inertia principle. The actuator has three supporting rods A, B and C, one fixed portion, one piezo-stack, two wedges, one friction head, two linear-type flexure hinges and four circular-type flexure

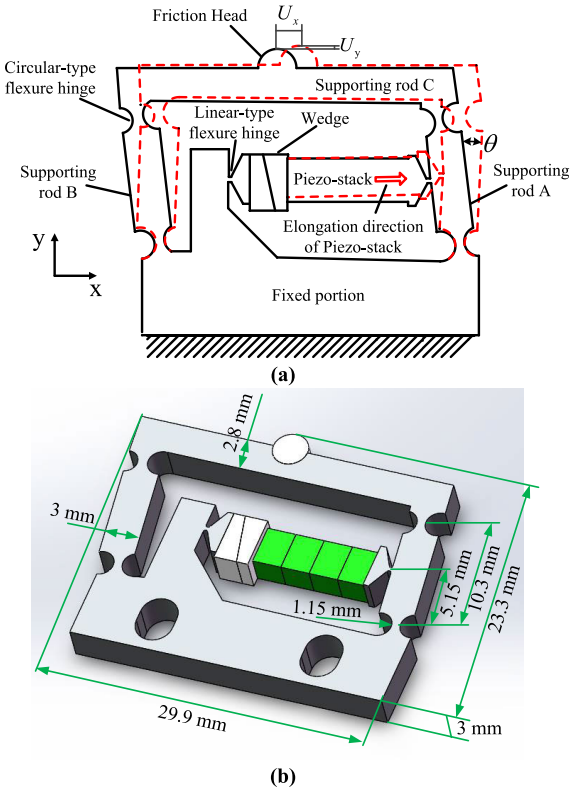

FIGURE 3. Structure of the actuator. (a) Schematic diagram; and (b) 3D model.

hinges. The circular-type flexure hinges act as the revolute pair, which has only one rotational degree of freedom. The supporting rods A and B are equivalent to the cranks A and B, and the supporting rod C and the fixed portion are equivalent to the linkages A and B. The piezo-stack works as the slide-block, which carries out reciprocating linear motion. The linear-type flexure hinge in the middle of the supporting rod A is equivalent to the linkage C, which plays a role in the regulation of motion transmission. Another linear-type flexure hinge between the fixed portion and the piezo-stack is used to decrease the concentrated pressure on the piezo-stack and thereby prevents damages to the piezo-stack. Two wedge blocks are used to adjust the pre-load between two linear-type flexure hinges. The friction head is glued to the middle of the supporting rod C. Except for one piezo-stack, two wedges and one friction head, all the portions are parts of a whole construction. When the piezo-stack is excited by a fixed voltage, the piezo-stack stretches to a certain length and pushes the supporting rod A to rotate around the revolute pair, and the friction head will have a larger lateral displacement U_x and a smaller vertical displacement U_y in the XY plane. The lateral displacement is mainly used to drive the actuator.

Figure.3(b) shows the three-dimensional model with dimensions of 27.6 × 21.6 ×3 mm^3, which including more intuitive structural information of the actuator. The piezo-stack is from NEC Inc. (AE0203D08H09DF; cross section: 2 × 3 mm^2; overall length: 10 mm; displacement at

TABLE 1. Material constants.

Material	AL7075	ZrO_2	Al_2O_3
Density(kg/m^3)	2810	6020	3850
Poisson's ratio	0.33	0.25	0.28
Elastic modulus(x10^{10}N/m^2)	7.2	32	34

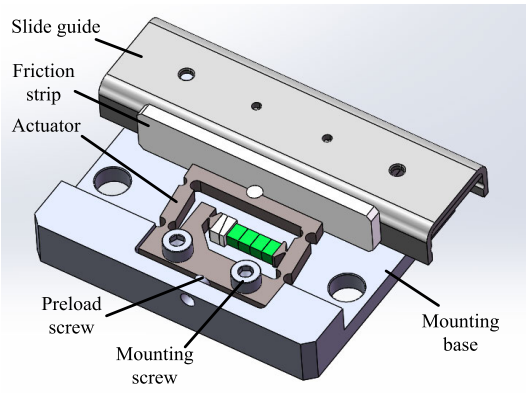

FIGURE 4. Moving platform driven by the designed actuator.

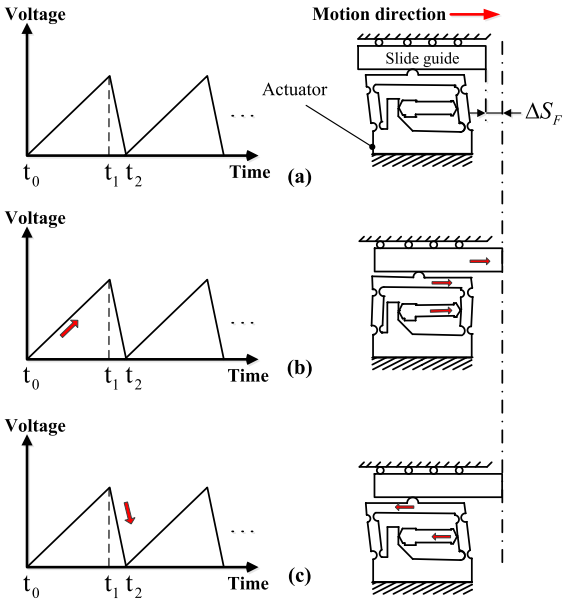

FIGURE 5. Mechanism of forward motion.

maximum voltage of 150 VDC: 9.1+/− 1.5 μm; stiffness: 22 N/μm; and generated force: 200 N). The whole construction and the wedges are made of aluminum alloy 7075. The friction head is made of ZrO_2. The relevant material coefficients are listed in Table 1.

The moving platform driven by the designed actuator is used to conduct the output performance test, as shown in Figure 4. The platform is comprised of an actuator, a friction strip, a slide guide, a mounting base, a preload screw and two mounting screws. The friction strip is connected to the side of the slide guide. Al2O3 is chosen for the friction strip,

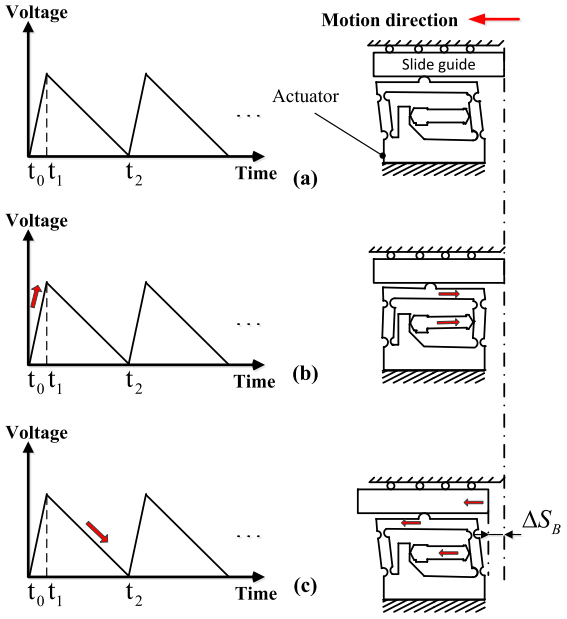

FIGURE 6. Mechanism of reverse motion.

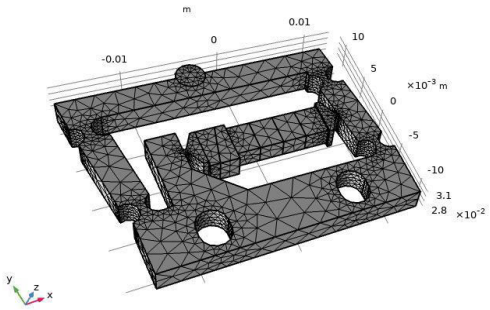

FIGURE 7. Finite element model of the designed actuator.

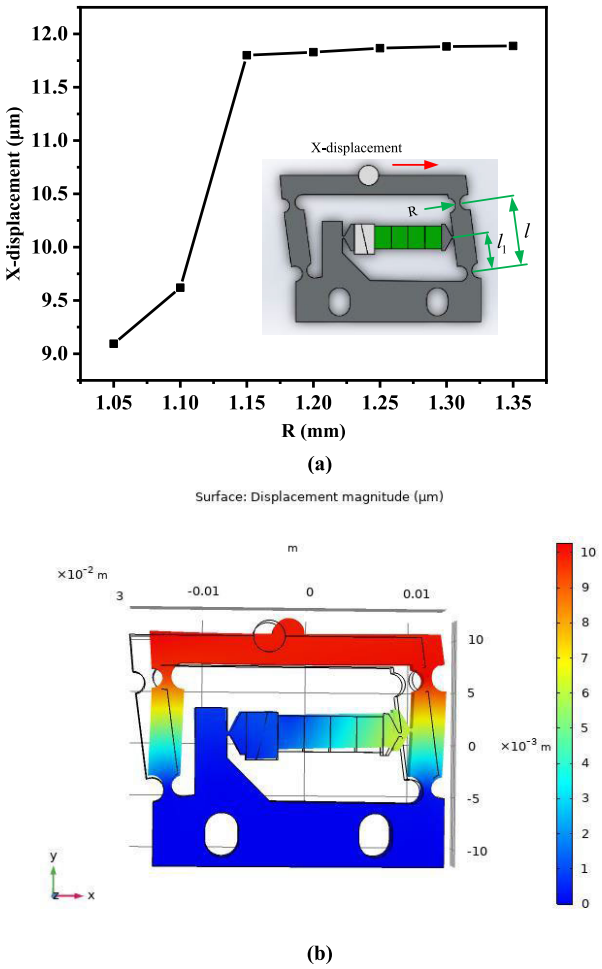

FIGURE 8. Static analysis simulation. (a) X-displacement of the actuator; and (b) R = 1.15 mm.

which forms one of the friction pairs with the friction head. A preload screw is used to adjust the normal force between the friction strip and the friction head. When the preload between the friction pair is adjusted to the appropriate value, the actuator is fastened to the mounting base by two mounting screws.

III. OPERATING PRINCIPLE

Figures 5 and 6 show the operating processes of positive and reverse motion in one cycle. Under the inertia principle, the designed actuator is driven by a saw-tooth wave voltage. A full cycle of the forward/reverse motion process can be divided into three phases. Let's take for example the forward motion. First, when the piezo-stack is not excited by any voltage, the actuator and the slide guide remain stationary. Then, under a linear slow ascending ramp voltage at the phase t_0-t_1, the piezo-stack drives the actuator, and the friction head rubs the slide guide to cause a forward movement of one step through frictional force. Third, as the voltage sharply drops to zero at the phase t_1-t_2, the piezo-stack quickly retracts to its initial position, and the slide guide remains stationary due to the inertia of the slide guide

As the entire cycle repeats, continuous motion in positive direction can be achieved.

IV. FINITE ELEMENT ANALYSIS

For accuracy of model calculations, second order quadrilateral cells are used to construct the actuator model, as shown in Figure 7. The finite element model contains 13450 elements and 3604 nodes. The corresponding material parameters of various portions are listed in section II. The fixed portion of the actuator is in a completely fixed state during the simulation. The following things are done in the process of finite element analysis: (1) calculation of the displacement of friction head in the XY plane to obtain the X-displacement magnification factor of the actuator; (2) calculation of the resonant frequency of the actuator to avoid interference from some of vibration modes.

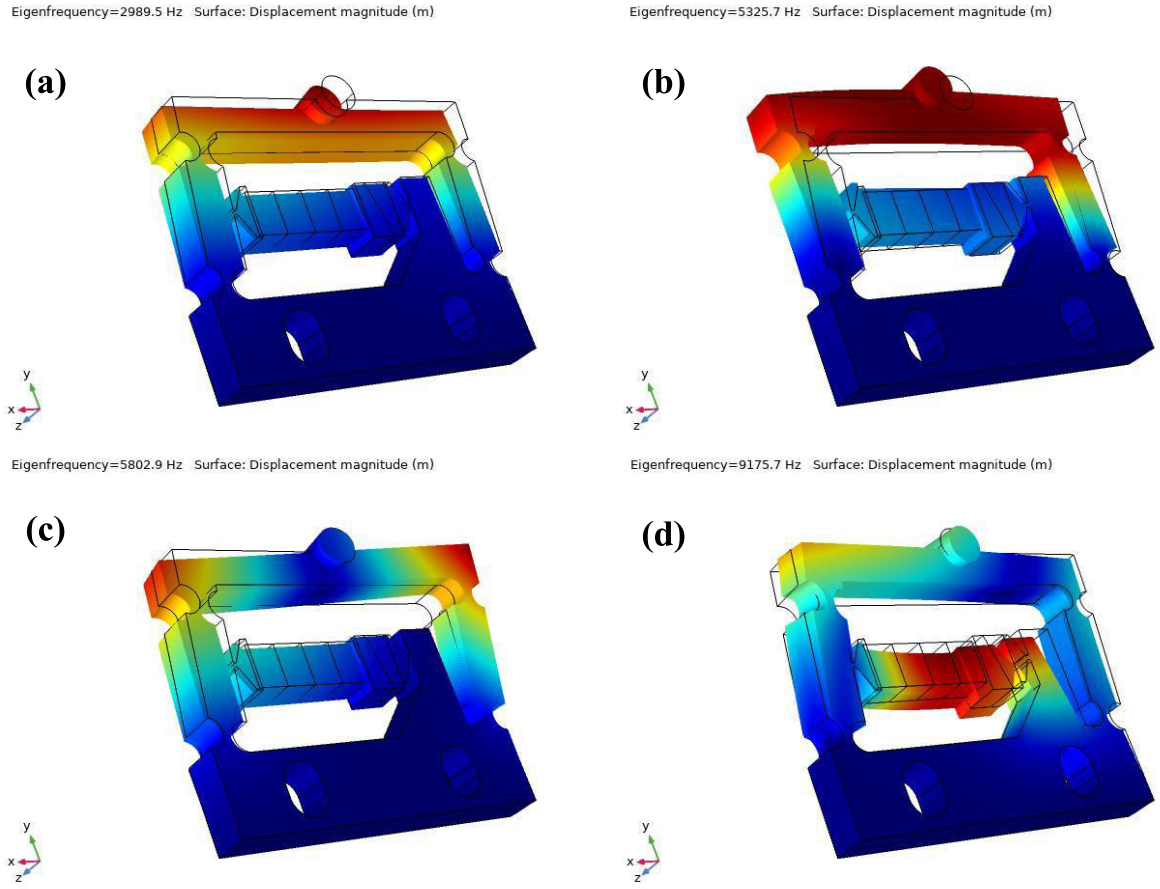

FIGURE 9. Modal analysis. (a) 2989.5 Hz. (b) 5325.7 Hz. (c) 5802.9 Hz. (d) 9175.7 Hz.

Due to the circular-type flexible hinge plays the role of rotation and the linear-type flexible hinge has a large stiffness in the X direction, the circular-type flexible hinge structure has a key impact on the displacement output of the actuator. Therefore, this section focuses on the design and analysis of the radius R of the circular-type flexible hinge. The influence of radius R of the circular flexible hinge on the output displacement of the actuator is obtained through the analysis of finite element software. The voltage amplitude is fixed at 100 V during the static analysis. As can be seen from Figure 8(a), the X-direction displacement of the output of the actuator increases sharply with the increase of radius R from 1.05 mm to 1.15 mm, and when the radius R exceeds 1.15 mm, the X-direction displacement gradually stabilizes. As the rotation stiffness of the circular-type flexible hinge decreases with the increase of radius R and the output displacement of piezo-stack reaches the maximum value, the output displacement of the actuator in the X direction reaches a stable value. Therefore, in order to ensure a certain stiffness of the actuator, the radius R value of the circular-type flexible hinge is set at 1.15 mm.

The displacement of the friction head in X direction in static simulation is about 11.8 μm, as shown in Figure 8(b). However, the stroke of the piezo-stack is approximately 6.1 μm at 100 V, and the X-displacement of the friction head can be calculated at 12.2 μm through the geometric relationship. The formulas for calculating the value of the X-displacement are shown in the following equations 2 to 4, where l and l_1 represent the length and half length of the supporting rod A respectively, with values of 10.3 mm and 5.15 mm respectively, θ indicates the rotation angle of the supporting rod A, S denotes the output displacement of the actuator in the X direction, and the output displacement S_1 of the piezo-stack is 6.1 μm. Therefore, the calculated value of the X-displacement of the friction head is in high agreement with the simulated value. The X-displacement magnification factor of the actuator is about 2.

$$S = l \sin\theta \tag{2}$$

$$S_1 = l_1 \sin\theta \tag{3}$$

$$l = 2l_1 \tag{4}$$

Under the inertia principle, the designed actuator operates in the non-resonant frequency range. Model analysis is required for the stable operation of the designed actuator and avoidance of interference from some vibration modes.

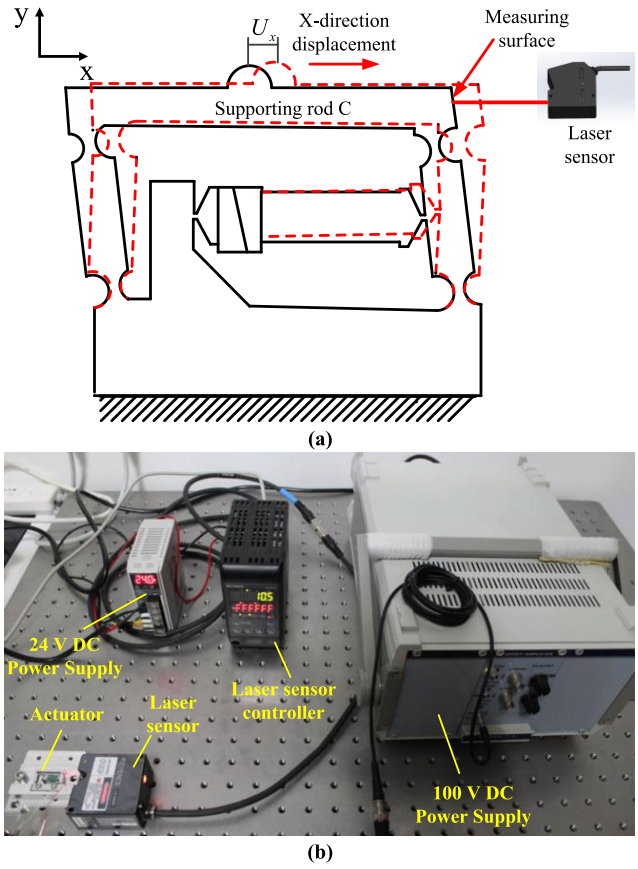

FIGURE 10. X-direction Displacement measurement system: (a) measurement diagram and (b) Measurement system of the experiment.

Figure 9 shows the model analysis results over the frequency range of 0 to 10 KHz. The resonant frequencies of the four modes are 2989.5 Hz, 5325.7 Hz, 5802.9 Hz and 9175.7 Hz, respectively. Hence, the working frequency of the designed actuator needs to be much lower than 2989.5 Hz.

V. EXPERIMENTS AND RESULTS

To verify the design and analysis of the actuator, the X-direction output displacement of the actuator was measured through experiments. The method of measuring the X-direction output displacement of the actuator is shown in the measurement diagram in Figure 10 (a). The X-direction displacement of the end face of the supporting rod C of the actuator is measured by the laser displacement sensor (LK-H020/LK-H150/LK-G5001P; Keyence Co., Osaka, Japan), that is, the output displacement of the friction head in the X direction. Figure 10 (b) shows the X-direction Displacement measurement system. A constant 100 V DC voltage source drives the actuator, and the other constant 24 V DC voltage source drives the laser controller and sensor. Table 2 shows the comparison between the two different calculation methods and the actual value of the experimental test. The results show that the actual measured value is slightly lower

TABLE 2. X-direction displacement results under different calculation methods.

Methods	X-direction Displacement(μm)
Theoretic analysis	12.2
Finite Element Method	11.8
Experiment	10.5

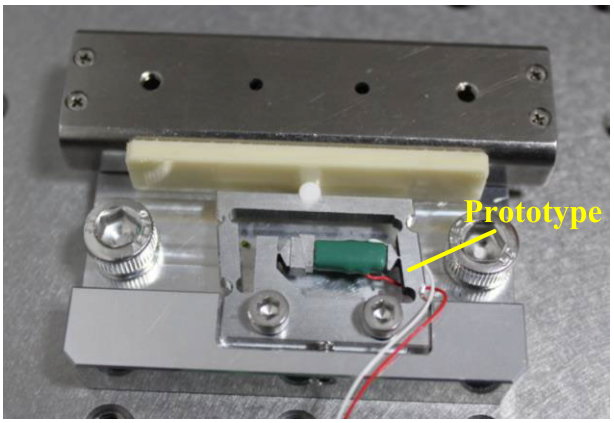

FIGURE 11. Actuator prototype and moving platform.

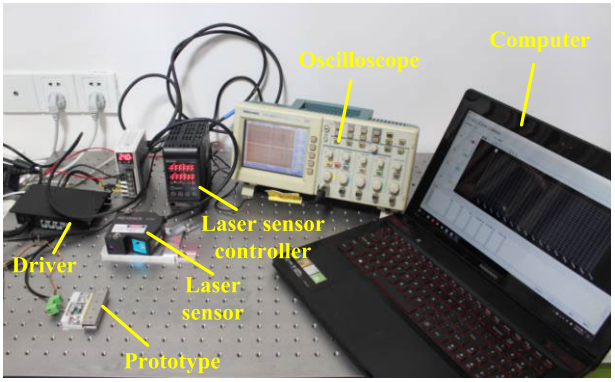

FIGURE 12. Experimental system for actuator.

than the theoretical analysis value and the finite element calculation value. The main reason is that there is a certain manufacturing error in the manufacturing process of the actuator. Through experimental verification, the correctness of the design and analysis of the actuator is proved.

For measuring the output characteristics of the designed actuator, we have created a prototype by electrical discharge machining and assembled the moving platform driven by the prototype, as shown in Figure 11. Figure 12 shows the experiment system for output characteristics. It consists of a moving platform, a driver, an oscilloscope, a laptop, a laser sensor and a controller system. The driver generates a saw-tooth waveform voltage required for the stable work of the actuator. The amplitude and frequency of the saw-tooth waveform

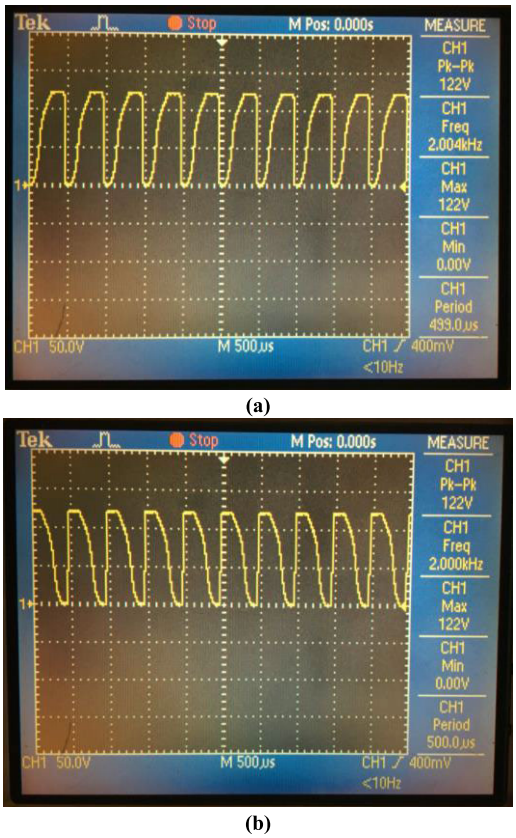

FIGURE 13. Saw-tooth wave voltages. (a) Positive and (b) negative.

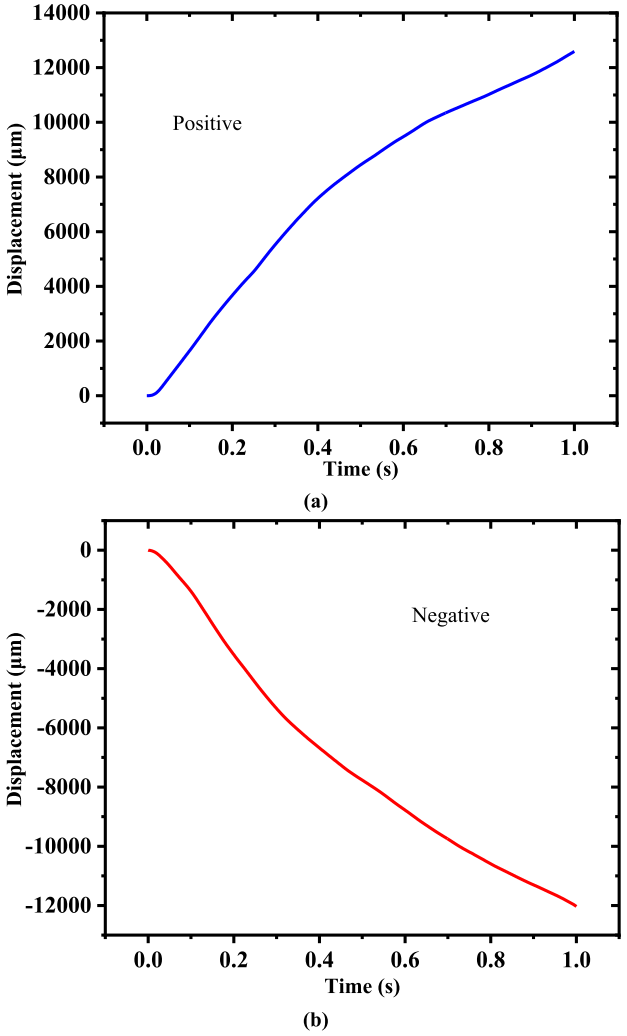

FIGURE 14. Displacement characteristics. (a) Positive and (b) negative.

voltage can be monitored by an oscilloscope (TDS2024; TEKTRONIX INC. BEAVERTON, OR U.S.A). The laser sensor and the controller are utilized to measure the output displacement and the speed of the moving platform. The measured experimental results are saved and recorded by a laptop.

The saw-tooth waveform voltages generated from the driver, as shown in Figure 13, are used to drive the positive and reverse movements of the platform. The amplitude and frequency of the saw-tooth waveform voltage are about 120 V and 2 KHz, respectively. The saw-tooth waveform voltage symmetry used to drive forward motion is 90%, while the voltage symmetry for reverse motion is 10%. Due to the capacitive properties of piezo-stack, the voltage has a slight harmonious distortion. However, this does not have much impact on the normal operating characteristics of the actuator. Therefore, two kinds of saw-tooth waveform voltages are selected as the driving voltages in the following experiments.

Through the continuous mode of the saw-tooth waveform voltages as shown in Figure 13, the continuous output characteristics can be obtained. To observe the output characteristics in detail, we set a sampling period of the controller to 0.1 ms. Figure 14 shows the continuous positive and negative output displacement characteristics within one second. The accumulated strokes of the moving platform within 1s time in the positive and reverse directions are 12590.9 μm and 11990 μm. The corresponding velocity curves within one second are shown in Figure 15. It is worth noting that the velocity first rises sharply, then falls, and finally flattens out. When the power is off at one second, the speed drops sharply with a period of shock attenuation. With the velocity dropping to zero, this phase can be defined as the shut-down response time. As the velocity rises from zero to the average velocity, this phase is defined as the start-up response time. The positive and negative average speeds are 12.59 mm/s and 11.99 mm/s, respectively, and the rate of velocity deviation is 4.9%. The start-up response times in positive and reverse directions are 14.4 ms and 8.1 ms, respectively, and the shut-down response times are 34.2 ms and 36.9 ms.

Step motion is usually intended for high precision. Unlike the continuous motion mode, the discontinuous mode as shown in Figure 16 is used to achieve step motion. The driving signal cycle of 3s includes a sawtooth waveform voltage of 0.5 ms, as shown in figure 15. When nine cycles of forward driving signals are completed, the accumulated step displacement is 45.71 μm. And with the same displacement,

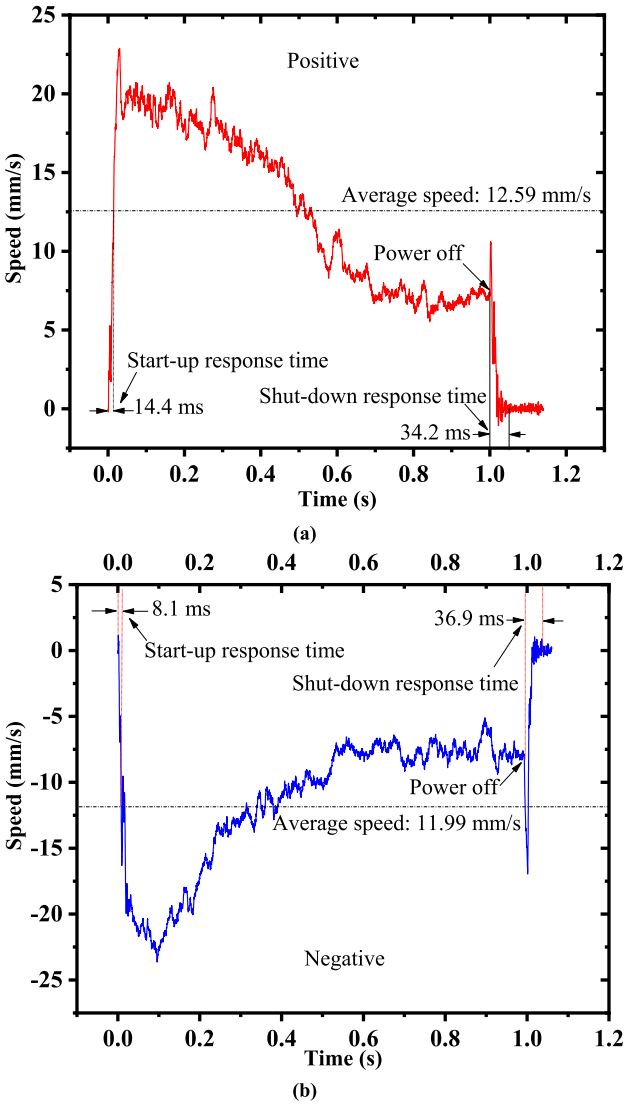

FIGURE 15. Speed characteristics. (a) Positive and (b) negative.

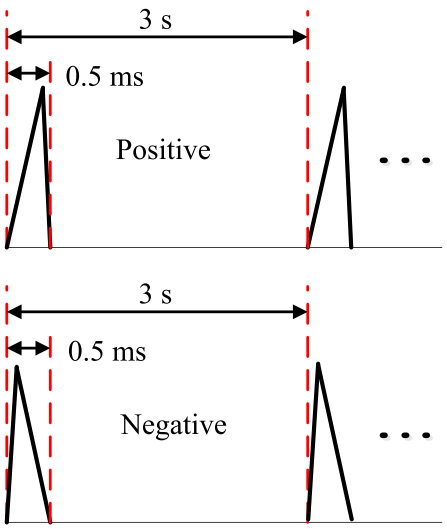

FIGURE 16. Pulse voltage.

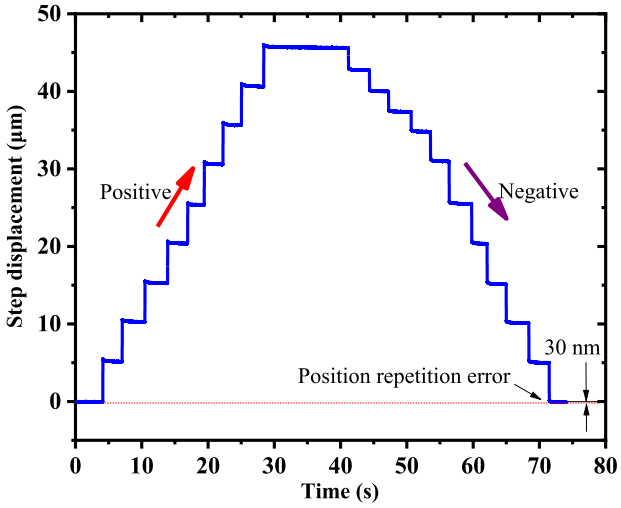

FIGURE 17. Step displacement characteristics.

11 cycles of reverse motion are completed due to the deviation between positive and reverse motion. The position repetition error in the positive and reverse directions is 30 nm, as shown in Figure 17. Therefore, the average step displacements in positive and reverse directions are 5.08 μm and 4.16 μm, respectively. To obtain a greater step displacement, we can increase the number of driving signal cycles to two or more.

The actuator bears a weight to simulate a constant load, as shown in Figure 18(a). The experimental results are shown in Figure 18(b). As the weight increases from 0 to 100 g, the average forward velocity decreases form 12.59 mm/s to 1.96 mm/s, and the average reverse speed decreases form 11.99 mm/s to 0.6 mm/s. As the weight increases further, the positive and reverse average speeds become extremely erratic. Therefore, the maximum load is determined as 100 g.

VI. COMPARISON AND DISCUSSION

Table 3 compares the speeds in this paper and those of previous actuators. According to the results, the rate of the speed deviation is reduced to 4.9%, which is much lower than those of previous actuators. Meanwhile, the forward and backward velocities have also increased, demonstrating that the novel piezo inertia actuator designed to imitate the motion mode of the steam train's transmission mechanism has a high speed and low deviations between positive and reverse speeds.

Due to the size limitation of the selected piezo-stack ($2 \times 3 \times 10$ mm^3), the load capacity of the actuator studied in this paper is lower than that of the previous actuator. The volume of piezo-stack selected by the previous actuator is about 8.3 times of that of piezo-stack in this study, and the maximum thrust is 4 times. In order to improve the thrust performance of the actuator designed in this study, a piezoelectric stack with a size of $5 \times 5 \times 20$ mm^3 can also be used. The corresponding actuator size has changed to

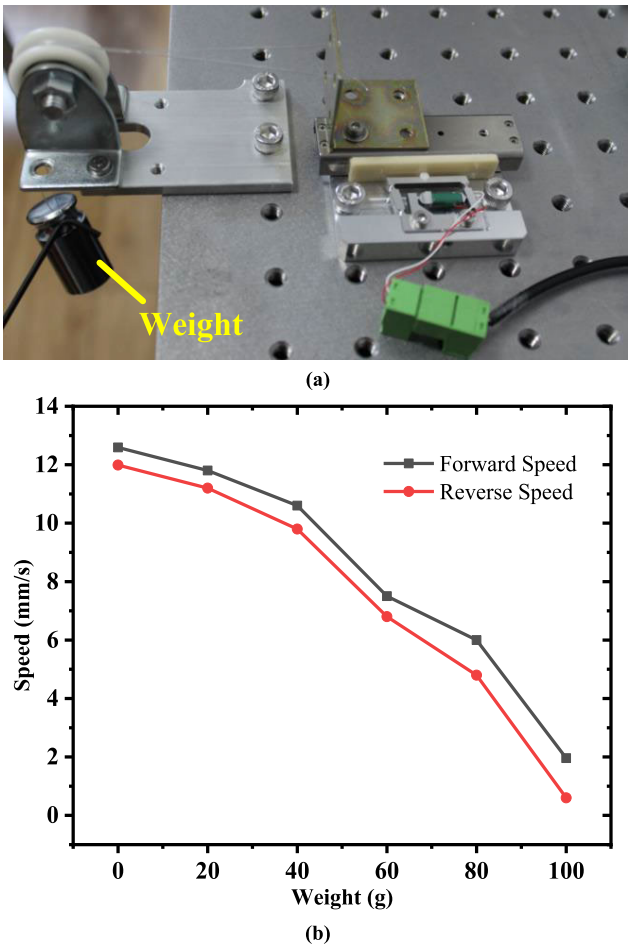

FIGURE 18. Load characteristics. (a) experimental setup and (b) characteristics curve.

TABLE 3. Comparison with other actuators.

Literature	[20]	[21]	[22]	[23]	This work
Forward speed (mm/s)	1.499	7.613	2.01	1.81	12.59
Reverse speed (mm/s)	1.18	10.058	2.34	2.45	11.99
Speed deviation	23.8%	27.67%	15.17%	30.05%	4.9%
Displacement in one step (μm)	19.1	4.7	0.89	4	5.08
Load(N)	2	2	3.8	0.1679	1
Size of Piezo-stack(mm^3)	5×5×20	5×5×20	5×5×20	/	2×3×10
Dimensions (mm^3)	/	62.3×29×5	54×44.2×9	10×9.7×8	27.6×21.6×3

37.6 × 21.6×5 mm^3, which has the advantage of compact structure compared with the previous actuators.

To obtain a smaller displacement of the actuator at each step, the following two methods can be used, such as: 1) the piezoelectric stack with a larger cross-section and a smaller length can be used to drive, but this will cause the speed of the actuator to decrease; 2) By adjusting the voltage, a smaller displacement is obtained at each step, but this will cause a decrease in thrust and speed.

Through the above discussion, no matter how to improve the speed, thrust and displacement of each step of the actuator, the actuator still has a low speed deviation and a compact structure.

VII. CONCLUSION

The study presents a novel piezo inertia actuator which imitates the motion mode of the steam train's transmission mechanism to decrease the deviation between positive and reverse velocities. Compared with the previous actuators, the positive and reverse velocities and the rate of the speed deviation have been obviously improved. The design compacts the structure of the actuator and easily achieves miniaturization, which is suitable for application. Under the sawtooth singal voltage of 120 V at 2 KHz, The average positive and reverse speeds within one second are 12.59 mm/s and 11.99 mm/s, respectively, and the rate of the velocity deviation is 4.9%. The start-up response times of the protype in positive and reverse directions are 14.4 ms and 8.1 ms, respectively, and the shut-down response times are 34.2 ms and 36.9 ms. In the step motion mode, the position repetition error in the positive and reverse directions is 30 nm. In addition, the maximum load is 100 g. This study confirms that the design of a novel piezo inertia actuator that imitates the motion mode of the steam train's transmission mechanism may provide a new concept for the design of an actuator with low speed deviations.

REFERENCES

[1] H. Chen, R. Nie, W. Han, and J. Qiu, "Improvement mechanism of energy conversion efficiency in ultrasonic motor with flexible rotor," *Ultrasonics*, vol. 120, Mar. 2022, Art. no. 106659.
[2] X. Hou, H. P. Lee, C. J. Ong, and S. P. Lim, "Development and numerical characterization of a new standing wave ultrasonic motor operating in the 30–40 kHz frequency range," *Ultrasonics*, vol. 53, no. 5, pp. 34–928, Jul. 2013.
[3] Y. Liu, S. Shi, C. Li, W. Chen, L. Wang, and J. Liu, "Development of a bi-directional standing wave linear piezoelectric actuator with four driving feet," *Ultrasonics*, vol. 84, pp. 81–86, Mar. 2018.
[4] W. Ren, L. Yang, C. Ma, X. Li, and J. Zhang, "Output performance simulation and contact analysis of traveling wave rotary ultrasonic motor based on ADINA," *Comput. Struct.*, vol. 216, pp. 15–25, May 2019.
[5] W. Ren, M. Yang, L. Chen, C. Ma, and L. Yang, "Mechanical optimization of a novel hollow traveling wave rotary ultrasonic motor," *J. Intell. Mater. Syst. Struct.*, vol. 31, no. 8, pp. 1091–1100, May 2020.
[6] R. Wang, L. Wang, B. Jia, J. Jin, and D. Wu, "Semi-analytical modeling and experimental evaluation on a novel standing wave rotary piezoelectric actuator driven by single-phase signal," *Mech. Syst. Signal Process.*, vol. 163, Jan. 2022, Art. no. 108177.
[7] M. den Heijer, V. Fokkema, A. Saedi, P. Schakel, and M. J. Rost, "Improving the accuracy of walking piezo motors," *Rev. Scientific Instrum.*, vol. 85, no. 5, May 2014, Art. no. 055007.

[8] D. Kang, M. G. Lee, and D. Gweon, "Development of compact high precision linear piezoelectric stepping positioner with nanometer accuracy and large travel range," *Rev. Scientific Instrum.*, vol. 78, no. 7, Jul. 2007, Art. no. 075112.
[9] R. J. E. Merry, N. C. T. de Kleijn, M. J. G. van de Molengraft, and M. Steinbuch, "Using a walking piezo actuator to drive and control a high-precision stage," *IEEE/ASME Trans. Mechatronics*, vol. 14, no. 1, pp. 21–31, Feb. 2009.
[10] X. Ma, J. Liu, J. Deng, Q. Chang, and Y. Liu, "A simplified inchworm rotary piezoelectric actuator inspired by finger twist: Design, modeling, and experimental evaluation," *IEEE Trans. Ind. Electron.*, early access, Jan. 23, 2023, doi: 10.1109/TIE.2023.3237900.
[11] M. Hunstig, T. Hemsel, and W. Sextro, "Stick–slip and slip–slip operation of piezoelectric inertia drives. Part I: Ideal excitation," *Sens. Actuators A, Phys.*, vol. 200, pp. 90–100, Oct. 2013.
[12] J. Li, H. Huang, and T. Morita, "Stepping piezoelectric actuators with large working stroke for nano-positioning systems: A review," *Sens. Actuators A, Phys.*, vol. 292, pp. 39–51, Jun. 2019.
[13] J. Deng, Y. Liu, J. Li, S. Zhang, and H. Xie, "Influence of multidirectional oscillations on output characteristics of inertial piezoelectric platform," *IEEE/ASME Trans. Mechatronics*, vol. 27, no. 5, pp. 4122–4131, Oct. 2022.
[14] J. Deng, W. Wang, S. Zhang, F. Lu, and Y. Liu, "An inertial bipedal piezoelectric actuator with integration of triple actuation modes," *Smart Mater. Struct.*, vol. 31, no. 11, 2022, Art. no. 115019.
[15] J. Li, S. Zhang, Y. Liu, J. Deng, and X. Ma, "A 3-DOF inertial impact locomotion robot constructed on four piezoelectric bimorph actuators," *Smart Mater. Struct.*, vol. 31, no. 9, Sep. 2022, Art. no. 095008.
[16] M. Xun, H. Yu, S. Zhang, Q. Chang, J. Deng, and Y. Liu, "A large-step stick-slip rotary piezoelectric actuator with high velocity under low frequency and small backward motion," *Smart Mater. Struct.*, vol. 32, no. 5, May 2023, Art. no. 055002.
[17] H. Huang and H. Zhao, "Forward and reverse movements of a linear positioning stage based on the parasitic motion principle," *Adv. Mech. Eng.*, vol. 6, Jan. 2014, Art. no. 452560.
[18] W. Sun, Z. Xu, K. Wang, X. Li, J. Tang, Z. Yang, and H. Huang, "An impact inertial piezoelectric actuator designed by means of the asymmetric friction," *IEEE Trans. Ind. Electron.*, vol. 70, no. 1, pp. 699–708, Jan. 2023.
[19] Z. Yang, X. Zhou, H. Huang, J. Dong, Z. Fan, and H. Zhao, "On the suppression of the backward motion of a piezo-driven precision positioning platform designed by the parasitic motion principle," *IEEE Trans. Ind. Electron.*, vol. 67, no. 5, pp. 3870–3878, May 2020.
[20] X. Li, X. Wang, W. Sun, K. Wang, Z. Yang, T. Liang, and H. Huang, "A compact 2-DOF piezo-driven positioning stage designed by using the parasitic motion of flexure Hinge mechanism," *Smart Mater. Struct.*, vol. 29, no. 1, Jan. 2020, Art. no. 015022.
[21] K. Wang, X. Li, W. Sun, Z. Yang, T. Liang, and H. Huang, "A novel piezoelectric linear actuator designed by imitating skateboarding movement," *Smart Mater. Struct.*, vol. 29, no. 11, Nov. 2020, Art. no. 115038.
[22] F. Qin, H. Huang, J. Wang, L. Tian, T. Liang, and H. Zhao, "Design and stepping characteristics of novel stick–slip piezo-driven linear actuator," *Smart Mater. Struct.*, vol. 28, no. 7, Jul. 2019, Art. no. 075026.
[23] X. Li, Z. Xu, W. Sun, D. Wei, H. Wu, and H. Huang, "A miniature impact drive mechanism with spatial interdigital structure," *Int. J. Mech. Sci.*, vol. 240, Feb. 2023, Art. no. 107933.

PINGPING SUN was born in Shanxi, China, in 1988. She received the Ph.D. degree in physics from Southeast University, Nanjing, China, in 2018.

She is currently a Full Lecturer with the School of Physics and Information Engineering, Jiangsu Second Normal University, Nanjing. Her current research interests include piezoelectric precision actuators, control theory, and lithium battery.

HUAN YU is currently pursuing the bachelor's degree with Jiangsu Second Normal University. Her main research interest includes electronic information.

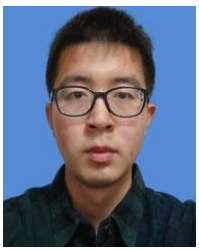

HAOZHEN ZHANG is currently pursuing the bachelor's degree with Jiangsu Second Normal University. His research interest includes electronic information engineering.